J Mater Sci (2007) 42:337–345
DOI 10.1007/s10853-006-1031-6

Sintering temperature depression in Al_2O_3 by mechanical milling

H. J. Goodshaw · J. S. Forrester · G. J. Suaning · E. H. Kisi

Received: 9 August 2004 / Accepted: 15 September 2005 / Published online: 14 November 2006

Abstract High-energy milling of Al_2O_3 with hardened steel milling media has confirmed that nanocrystalline powders are readily formed. At a ball to charge mass-ratio of 20:1, the crystallite size falls below 30 nm in just 2 h and below 15 nm in 4 h. The as-milled powders are contaminated with Fe which increases linearly with increased milling time, reaching ~10 wt% after 16 h. The HCl leaching process of Karagedov and Lyakhov [Karagedov and Lyakhov (1999) Nanostruct Mater 11(5):559] was found to remove a large proportion of the Fe, but residual Fe was found with XRF analysis. Milled and leached samples show significant sintering temperature depression to approximately 1100 °C and produce sintered densities greater than 94% without the application of pressure. Milling induced lattice expansion of the Al_2O_3 is observed which we posit to be due to defect formation rather than Fe absorption. The respective roles of small crystallite size and lattice defects in reducing the sintering temperature are discussed.

Introduction

It is widely held that considerable advantages would arise from the reduction in the sintering temperature of Al_2O_3. These include reduced costs, finer sintered grain sizes, and the ability to co-fire Al_2O_3 with materials of lower melting point. To achieve high densities in alumina components, compacted alumina powder is normally sintered above 1700 °C [2, 3]. It is known that the sintering temperature may be depressed by several hundred degrees through the addition of dopants, or beginning with a very fine initial particle size [4].

The doping of alumina for sintering temperature reduction entails adding oxides in amounts usually less than 1% but sometimes as great as 3%. Dense alumina can be sintered below 1400°C with small additions of MnO_2 and/or TiO_2 [2]. Other dopants shown to reduce the sintering temperature include Cu_2O, CaO and SiO_2. Dopants decrease the densification temperature either through the formation of a grain boundary film of liquid eutectic, or by creating defects that enhance bulk diffusion rates [5]. The highest densities have been achieved when the dopants are added in combinations [6, 7]. A disadvantage of dopants is their often deleterious effect on the physical and chemical properties of Al_2O_3 [5]. Alumina has long been used as a biocompatible material. Regulatory influences and inherent conservatism within the biomedical field substantially limit variance from previously tested and utilised materials. As such, new, or broad variations from existing dopant combinations are prohibitively difficult to justify and implement.

Reduction of the starting particle size in pure Al_2O_3 has been achieved using several specialised techniques, the most common of which is sol-gel processing [e.g. 8, 9]. Others include the injection of aluminium metal powder into the plasma jet of a thermal plasma reactor which results in the in-flight oxidation of nano-sized alumina (< 30 nm diameter) [10]. Solution based

H. J. Goodshaw · J. S. Forrester (✉) · G. J. Suaning · E. H. Kisi
School of Engineering, University of Newcastle, Callaghan, NSW 2308, Australia
e-mail: Jenny.Forrester@newcastle.edu.au

combustion synthesis has also resulted in nano-sized alumina. Citric acid and ammonia added to an aqueous solution of $Al(NO_3)_3$ with the application of heat caused the then dried powder to catch fire, resulting in an amorphous alumina. X-ray diffraction (XRD) patterns of powders calcined at 700 °C show some recrystallisation, and at 1200 °C a crystalline powder was formed [9]. In other work, Al wire was exploded using pulsed wire evaporation to produce Al particles with diameters of 80–120 nm as a starting material [11]. Hydrolysis was then used to produce aluminium hydroxide gel, and dehydration produced γ-Al_2O_3. Although practical on the laboratory scale, scaling up these techniques for industrial applications is questionable.

High-energy mechanical milling has been shown to produce nanometre sized particles in many materials including Al_2O_3. Karagedov and Lyakhov [1] milled Al_2O_3 using a planetary mill achieving estimated grain sizes of 18–40 nm. It was found that milled powders have enhanced sintering kinetics enabling 92% dense materials with fine grains (0.1–0.2 μm) to form after sintering at only 1200–1270 °C, considerably below the 1400°C observed using doping. In other related work, Goldsby [12] sintered milled mixtures of nanometre and micrometre sized powders at 1500 and 1600°C to study the high temperature creep behaviour of powders with different crystallite sizes. Strains as high as 0.65% were measured in a powder with 90% <28 nm grains and 10% μm sized grains. The lowest creep strains were measured in a 100% micron sized material. The best physical properties were gained from powders with a high volume fraction of nanometre sized grains.

Two problems commonly associated with mechanically milled powders are contamination and agglomeration. Alumina has a very high hardness, and mechanical milling is likely to be associated with contamination from the milling media. Some journal contributions concerning mechanical milling acknowledge contamination however most ignore it [12]. We have found contamination to be an integral part of the technique. Karagedov and Lyakhov [1] have demonstrated that Al_2O_3 powders milled with Fe-based media can be de-contaminated by boiling the milled powder in a 3–5% HCl solution. No spectroscopic data or limits governing residual Fe were given, however to the detection limit of their XRD no Fe was observed. The amount of residual Fe was later corrected to 1.5% [13]. Also, these authors state that milling Al_2O_3 in the same experimental arrangement under an inert atmosphere reduces the interaction between the Fe and Al_2O_3. It is suggested that residual Fe can be reduced to 0.02%.

The second problem, agglomeration, promotes uneven sintering which sometimes results in mechanically weak and porous products. Alumina powder particles in agglomerates are known to increase the volume and size of pores in the green compact [4]. This causes a decrease in the densification rate in the sintered compact. To achieve the highest densities, the agglomeration needs to be controlled.

The present paper reports on a re-examination of the use of high-energy mechanical milling of Al_2O_3 using hardened steel milling media as a means to reduce sintering temperatures. The de-contamination procedure of Karagedov and Lyakhov [1] was tested. Changes in the structure of the powder during milling and sintering are discussed, and depression of the sintering temperature to 1130 °C or lower seems attainable.

Experimental

Commercial Al_2O_3 powder (99.9%, Aldrich, Australia) was milled in a hardened steel vial using hardened steel grinding media, with a ball:powder ratio of 20:1. Milling was conducted in a SPEX8000 mixer/mill for 1–16 h. Evolution of the powders was monitored by XRD using a Philips 1710 powder diffractometer using Cu K_α radiation and fitted with a graphite monochromator. XRD scans were collected in the range 10–90° 2θ, a step size of 0.04° and a step counting time of 2 s.

De-contamination of milled powders was carried out using a HCl solution in a modified form of the procedure of Karagedov and Lyakhov [1]. The HCl solution was simultaneously stirred and heated on a hot-plate to aid in the dissolution of the Fe. The powder was separated from the solution by filtration through fine filter paper, and then oven-dried. To determine the presence of residual Fe, X-ray fluorescence (XRF) elemental analyses were conducted using a Spectro X-Lab 2000 spectrometer on samples milled for 16 h, cleaned using the procedure described, and absorbed into a lithium borate flux.

For sintering tests, Al_2O_3 powders were uniaxially pressed at 200 MPa into compacts approximately 6 mm thick. Two methods were used to examine sintering of the milled powders. Firstly, dilatometer scans were recorded in air. Samples were heated at 2.5 °C/min from 30 to 1410 °C, soaked for 15 min then cooled at the same rate as heating. To determine if the de-contamination procedure influenced the sintering characteristics of the alumina samples, dilatometer tests of Al_2O_3 that was treated the same way but without milling were also recorded. In addition, to determine if residual Fe influenced the sintering behaviour, a dilatometer scan

was recorded of alumina powder with a 3 wt% Fe addition that was milled for 15 min to promote mixing. Samples were also heated at 5 °C/min to 1130 °C and soaked there for 12 h, then heated to 1410 °C for a further 2 h, and cooled at the same rate as during heating. Second, pressed compacts were sintered at 1200, 1300 and 1400 °C for 4 h in a conventional high temperature furnace in air to provide scanning electron microscope (SEM) samples and to allow the measurement of sintered density. Sintered samples for SEM were polished with 1 μm diamond paste.

Secondary and back-scattered electron images were obtained using a Philips XL30 SEM, operated at 15 kV. When required, elemental fluorescent X-ray spectra were collected using an Oxford ISIS Si/(Li) energy dispersive spectroscopy (EDS) detector. Powders at several stages of milling were embedded in epoxy resin and polished to a 1 μm finish for SEM examination.

Rietveld refinements using the XRD patterns were performed using the computer program LHPM [14]. The global parameters refined were the zero point, scale factor and four coefficients of a background polynomial. The following additional structural and instrumental parameters were refined:

i. The lattice parameters (a and c).
ii. The full width at half maximum of the Lorentzian component of the Voigt peak shape function (k) so that crystallite size could be examined.
iii. The Gaussian half-width parameter, U, as it is associated with internal strains in a sample.

The instrumental variables, i.e. the asymmetry parameter and the peak width parameters V and W, were fixed at 0.005, –0.0027 and 0.0036 and respectively, following refinements using data recorded from a NIST Al_2O_3 standard (1976).

Results

Milled alumina prior to cleaning

XRD patterns showing the effects of high-energy milling on Al_2O_3 milled from 0 to 16 h are shown in Fig. 1. After 2 h the peaks of the corundum (α-alumina) crystal structure have broadened significantly. At greater than 4 h, significant intensity not attributable to Al_2O_3 appears at approximately 45 and 83° 2θ, due to increasing contamination by Fe. This is expected due to the high hardness of Al_2O_3. Visually, after 16 h of milling the Al_2O_3 powder appears quite black from Fe contamination.

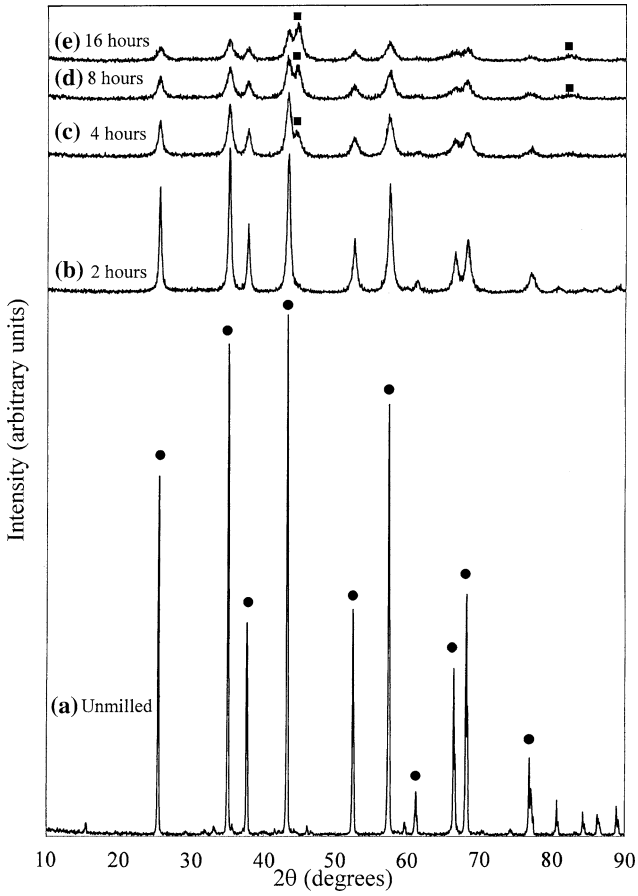

Fig. 1 Cu K_α X-ray diffraction pattern from Al_2O_3 milled for 0–16 h (● = Al_2O_3 diffraction peaks, ■ = Fe diffraction peaks)

After milling for 16 h, the diffraction peaks are very broad, indicating a small crystallite size. These were examined using Rietveld refinement and subsequent interpretation of the peak width parameters using the Scherrer equation, as shown in Fig. 2. We have relied here on the Secθ dependence of particle size broadening and an assumed Lorentzian peak shape for the crystallite size component of the broadening [15]. The initial crystallite diameter is ~425 nm, and after 2 h it has reduced to 30 nm. Further milling reduces the size to 13 nm, but the majority of the size reduction (to 15 nm) occurred within the first 4 h with little significant reduction thereafter.

Other refined parameters for the milling series are shown in Table 1. Changes in the lattice parameters a and c are shown in Fig. 3. Both increase with milling time by approximately 0.3%.

Al_2O_3 and Fe phase proportions in each milled powder were calculated from the Rietveld refinements using the method devised by Hill and Howard [16]. The results are shown in Fig. 4. There is an approximately linear increase in the wt% of Fe with milling

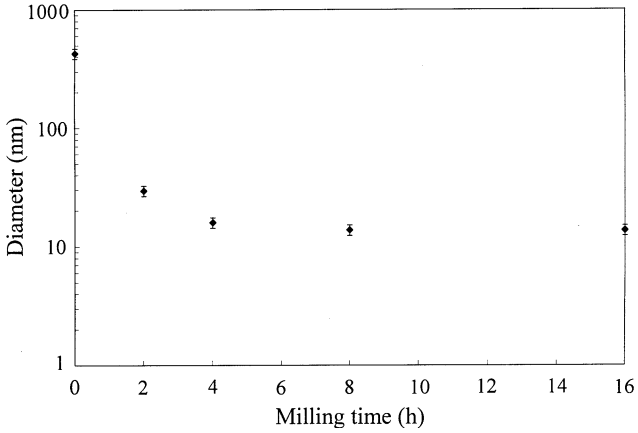

Fig. 2 Crystallite diameter as a function of milling time determined from X-ray diffraction line broadening. Error bars are plotted at one combined standard deviation of the observed Lorentzian half-width parameter k_{obs} and the instrumental Lorentzian half-width parameter k_i

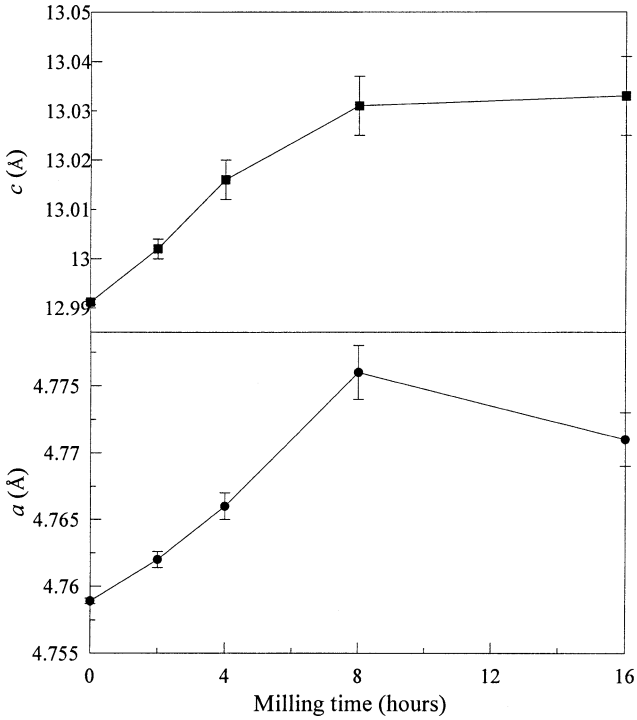

Fig. 3 Lattice parameters a and c of Al_2O_3 as a function of milling time. Error bars are plotted at one standard deviation of the observed lattice parameters. The lines are to guide the eye

time. Although the size of the diffraction peaks in Fig. 1 appears to indicate a large contribution by Fe in the sample milled for 16 h, phase analysis shows that it is just above 10 wt%.

Back-scattered SEM micrographs of Al_2O_3 powder before and after milling are shown in Fig. 5 and highlight differences in the particle size and Fe contamination. Figure 5a shows an unmilled Al_2O_3 with particles of approximately 50 μm in diameter. The particles are uniform in concentration as expected. Figure 5(b, c) shows that after 16 h of milling two sizes of agglomerates are present in this powder. Fine and dense hard agglomerates (0.2–4 μm) composed of many Al_2O_3 crystallites are loosely packed into large (10–100 μm) soft agglomerates. Closer inspection (Fig. 5c) shows that these agglomerates are an intimate mix of Al_2O_3 (dark) and Fe (white).

Milled alumina following cleaning

The HCl concentration required to dissolve the Fe contaminant in each sample was calculated using the phase proportions from the Rietveld refinements discussed above and a 10% excess. This de-contamination had the additional benefit of breaking up some of the soft Al_2O_3 agglomerates (Fig. 5d). Three things are apparent. First, not all of the Fe has gone. Remnants (white areas) can be seen in Fig. 5d. Second, it is apparent that the agglomerates are not as tightly packed together as in Fig. 5b. Third, it is now possible to discern some of the substructure of the hard agglomerates at the 0.2–1 μm level.

The effects of de-contamination on the sample milled for 16 h are shown in the XRD patterns in Fig. 6. This sample was chosen because it was the last in the series, and had the highest Fe contamination. Fig. 6a repeats the XRD pattern from Fig. 1e, but now as the initial pattern in the de-contamination series. Fig. 6b shows that following cleaning, the major Fe

Table 1 Refined lattice parameters, Lorentzian FWHM, Gaussian FWHW, estimated crystallite size, and R_B factors

Milling time (h)	a(Å)	c(Å)	Lorentzian FWHM	Gaussian FWHM (U)	Crystallite size (nm)	R_B (Al_2O_3)
0	4.7589(2)*	12.9912(5)	0.053(1)	0.030(2)	426.7	4.62
2	4.7620(6)	13.002(2)	0.333(7)	0.61(4)	29.4	2.97
4	4.766(1)	13.016(4)	0.59(1)	1.4(1)	15.9	2.31
8	4.776(2)	13.031(6)	0.67(2)	1.2(2)	13.8	2.76
16	4.771(2)	13.033(8)	0.68(6)	1.1(3)	13.7	2.85
16, sintered 1300 °C, 4 h	4.76280(8)	13.0015(3)	0.0410(7)	0.0132(6)	1015.4	5.34

* The number in parentheses refers to the right-hand digit and represents the standard deviation estimated in the Rietveld analyses

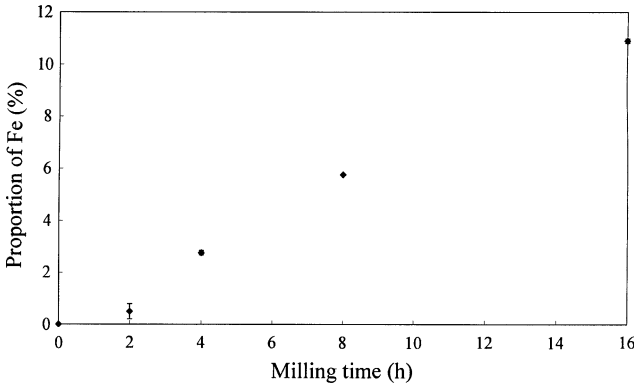

Fig. 4 Percentage of Fe in the Al_2O_3 powder with milling time calculated from the Rietveld refinements. Error bars indicate one estimated standard deviation

diffraction peak at ~45° 2θ is eliminated, indicating that the majority of the free Fe has been removed. The XRD pattern after the powder was pressed into a pellet then sintered at 1300 °C for 4 h is shown in Fig. 6c and is discussed later. Once again no Fe (or related oxides) is seen. The powder remained light greyish in colour following cleaning, an indication that some Fe remains. XRF analyses of the cleaned powder showed approximately 2 wt% Fe. This residual Fe can be looked upon as an inadvertent doping with Fe.

Sintering

Examples of dilatometry results are shown in Figs. 7 and 8. Samples heated at 2.5 °C/min to 1410 °C are shown in Fig. 7. The unmilled sample shows little compaction until 1100 °C and sintering has only partly completed at 1410 °C. In the milled and cleaned sample there is a considerable amount of pre-sintering densification all through the heating ramp to ~750 °C. Beyond 750 °C the densification rate increases gradually to a maximum in the range 1100–1300 °C. The slope decreases above 1300 °C indicating that the majority of sintering has been completed at lower temperatures. The sample milled for 15 min with 3 wt% Fe added shows similar sintering behaviour to

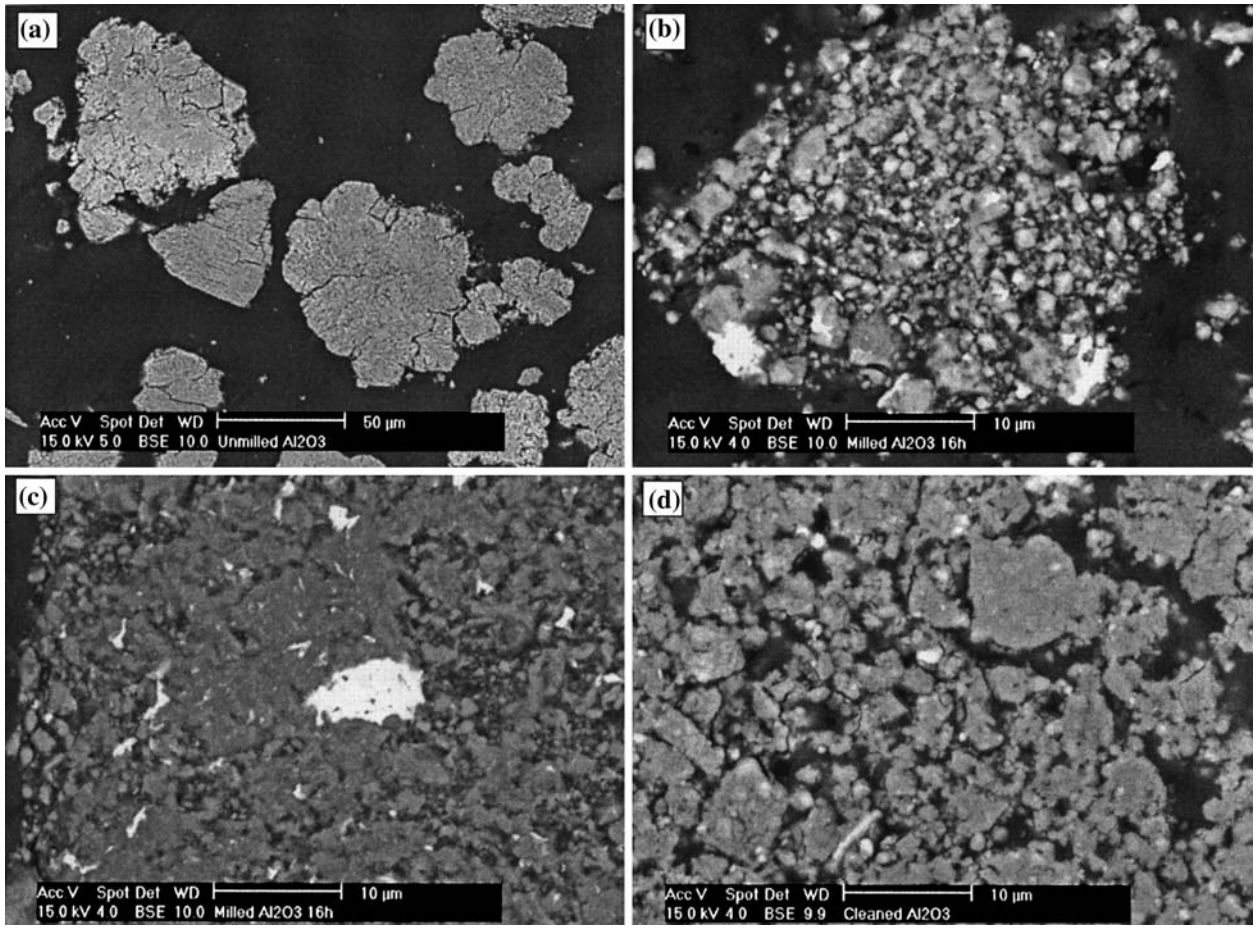

Fig. 5 Back-scattered electron micrographs of (**a**) unmilled Al_2O_3, (**b**) an agglomerate after milling for 16 h, (**c**) a cross-section of an agglomerate after milling for 16 h, and (**d**) a sectioned sample following milling and cleaning

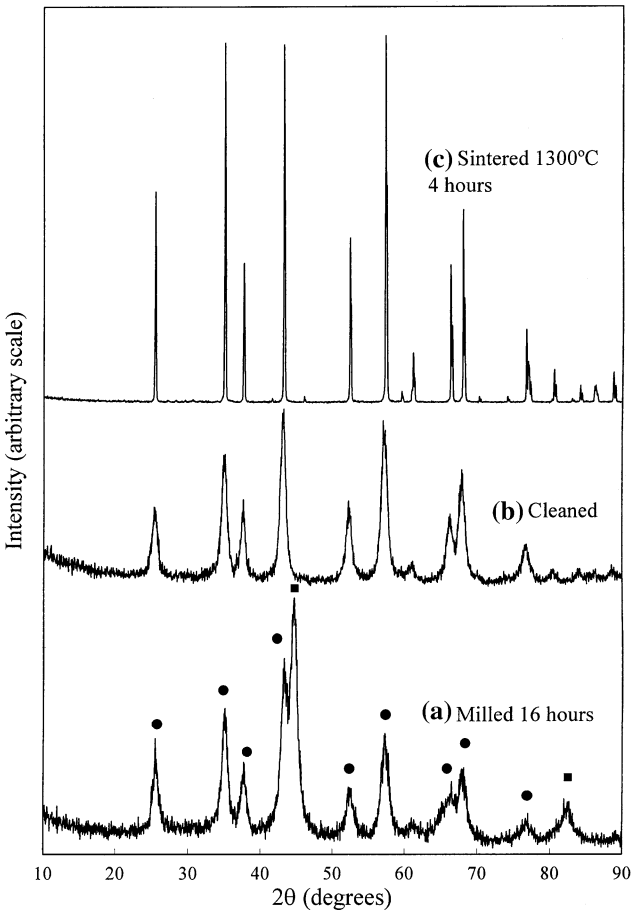

Fig. 6 XRD patterns showing the effects of de-contamination following milling for 16 h (● = Al_2O_3 diffraction peaks, ■ = Fe peaks) (**a**) after milling for 16 h, (**b**) after cleaning with HCl, (**c**) sintered for 4 h at 1300 °C (intensity scale decreased by a factor of 5 for comparison with other XRD pattern in this figure)

the unmilled sample except that compaction begins earlier, at around 950 °C. It is evident that sintering is far from complete in the unmilled samples. Indeed, inspection of the samples following the dilatometer tests showed that the milled samples were monolithic whereas the other samples remained powdery. Although Fig. 7 shows that sintering was not yet complete, density measurements showed that the sample milled for 16 h and cleaned with HCl had attained 94% of theoretical density. To achieve these densities in Al_2O_3, temperatures of greater than 1450 °C are normally required. For comparison, the unmilled alumina attained 87% of theoretical density, and the sample mixed with Fe attained 81% of theoretical density after an identical firing cycle.

Isothermal dilatometry was also conducted. Displacement versus temperature data for a sample held at 1130 °C for 12 h, then heated to 1410 °C for a further 2 h is shown in Fig. 8a, and displacement versus

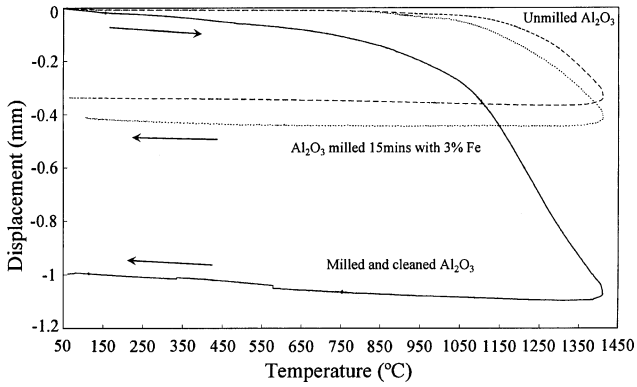

Fig. 7 Dilatometer tests of unmilled alumina (dashed line), milled and cleaned alumina (solid line), and alumina with 3wt% Fe added (dotted line) during heating from 50 °C to 1410 °C and during the cooling to 50 °C

time in the same test is shown in Fig. 8b. The steep slope indicates significant sintering at 1130 °C which has not completed after 12 h. The residual negative slope towards the end of the hold at 1130 °C (Fig. 8b) confirms that sintering at 1130° is continuing, albeit very slowly. With the temperature increase to 1410 °C

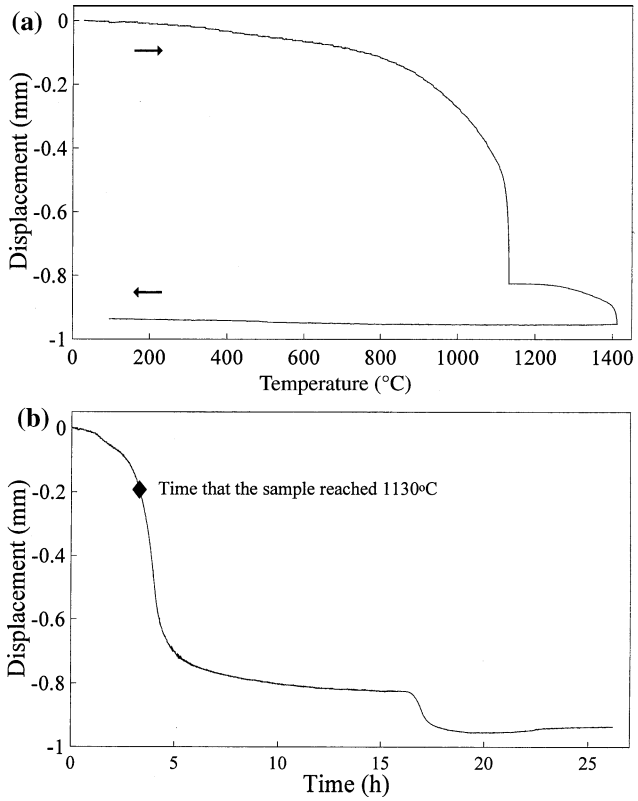

Fig. 8 Dilatometer test showing milled and cleaned alumina heated at 5°/min to 1130 °C and soaked there for 12 h, then heated at the same rate to 1410 °C and held there for 2 h

there is some additional sintering. This sample attained 96% of theoretical density.

The structure of the sintered ceramics was investigated using Rietveld analysis of the XRD patterns (Fig. 6c), and the results are given in Table 1. The diffraction peak width is in fact less than for the as-received powder. The Scherrer equation was applied, and the mean crystallite size was estimated as 1015 nm.

The microstructure of sintered alumina is shown in the SEM micrographs of Fig. 9. Fig. 9a shows the surface of a sintered Al_2O_3 doped with MgO (0.23%), MnO_2 (2%) and TiO_2 (1.8%) and sintered at 1475 °C for comparison with the samples in this work. Fig. 9b shows the surface of an alumina sample processed by mechanical milling and sintered at 1300 °C. The grain size in Fig. 9b is far smaller than that of the doped sample in Fig. 9a. The grains of the sample produced by milling are tabular in stark contrast to the equiaxed grains of the doped sample and there appears to be a small amount of surface porosity. Figure 9(c, d) shows the fracture surface of an alumina compact sintered at 1300 °C. This again shows the unusual grain shapes in these samples. The compacts appear to be dense with little porosity, and the fracture is transgranular.

Discussion

Nanocrystalline Al_2O_3 can readily be produced by mechanical milling, as evidenced by XRD peak broadening which is governed by the size of the diffracting domain (Fig. 1) and subsequent crystallite size analysis (Fig. 2). The values in Table 1 show that the crystallite size is approximately 14 nm in the powder milled for 16 h. Longer milling times than those performed here are likely to gain few benefits, as most of the size reduction occurs within 4 h of milling. Apart from the practical aspects of milling for shorter times, there is the benefit of less Fe contamination in the milled product.

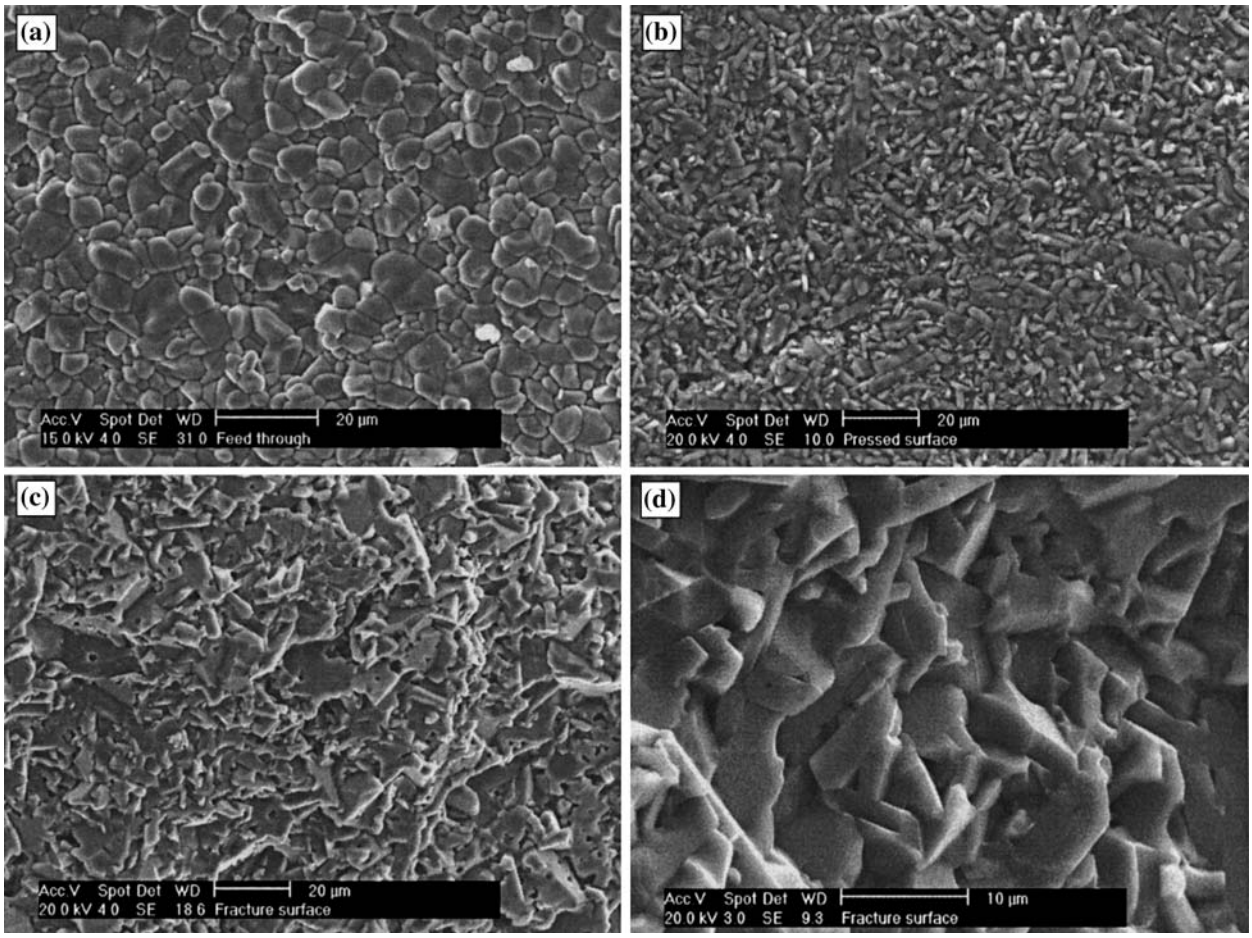

Fig. 9 Secondary electron micrographs of a sintered Al_2O_3 (**a**) typical surface microstructure of sintered Al_2O_3 doped with MgO, MnO_2 and TiO_2 and sintered at 1475 °C, (**b**) surface of Al_2O_3 sintered at 1300 °C, (**c**) fracture surface of the sintered compact, (**d**) higher magnification micrograph of a fracture surface

Phase quantitation showed that Fe contaminates the Al_2O_3 approximately linearly with milling time (Fig. 4). It is reasonable to assume there are benefits in achieving small crystallite sizes with minimal contamination. The decontamination procedure of Karagedov and Lyakhov [1] removes any trace of Fe observable by XRD (Fig. 6b), however some residual Fe remains (XRF and Fig. 5d). Extended leaching periods and other small variations in the cleaning procedure did little to reduce the Fe content further. Residual Fe appears to be completely encapsulated by the Al_2O_3 so that the HCl cannot access it. Perhaps some kind of physical de-agglomeration (e.g. mild grinding) may be necessary. We are currently performing similar work using an alumina vial and milling balls.

During the milling and sintering process the alumina remains in the α-Al_2O_3 form, but the lattice expands (Fig. 3). This may be due to the introduction of vacancies and other defects, or Fe absorption into the Al_2O_3 lattice. Calculations from the data in Fig. 3 show that there is approximately 0.3% increase in the lattice parameters after 16 h of milling. Attributing this increase entirely to Fe incorporation into the Al_2O_3 crystal structure would require 5.5–7.6 wt% Fe_2O_3 (assuming Vegard's Law holds). However, after cleaning we can observe a few percent of *metallic* Fe in the SEM (Fig. 5d). This iron becomes incorporated into the Al_2O_3 during sintering since no new phases are observed in either XRD or SEM data. If substantial Fe was already present in the Al_2O_3 crystal structure after milling, we would expect the lattice to expand further as the metallic Fe visible in Fig. 5d is absorbed. However, instead we observe a lattice contraction from the milled to the sintered state. Further, an estimate of the Fe content of the Al_2O_3 (2.2 wt% Fe_2O_3) based upon the as-sintered lattice parameters (Table 1) is in reasonably good agreement with the results of XRF total Fe analysis prior to sintering (3.2 wt% Fe_2O_3). Accordingly, most of the milling induced lattice parameter increase cannot be attributed to Fe incorporation into the lattice. Much of the lattice parameter increase must be attributed to defects produced by the milling process. Other researchers have noted changes in lattice parameters, but it has generally been entirely attributed to Fe incorporation. For example, 9 wt% Fe was measured after 8 h of milling yttria-alumina combinations, and in this case it was said to be completely responsible for the lattice expansion [17].

The dilatometry tests show a significant reduction in the sintering temperature of milled alumina, to below 1200 °C. Fig. 8 shows that when a sample is soaked at 1130 °C for 12 h, there is initially a steep increase in slope which indicates that a large amount of sintering is occurring. After about 5 h, the sintering rate slows. It is important to note, however, that the sample continues to sinter at this temperature. The microstructures of milled/cleaned /sintered samples are very promising. The grain size is very fine (~1 μm). In addition, the sintered densities are high (up to 96%). SEM micrographs (Fig. 9) indicate that the porosity appears to be closed pores within grains.

An interesting effect noted during the dilatometry was that there is compaction at very low temperatures, almost immediately that the temperature is increased in milled samples (Fig. 7). The indications are that sintering below 1000 °C is a possibility, by using very long soak times. This is in stark contrast to the unmilled alumina where there is little compaction at low temperatures. It is uncertain whether the low temperature compaction is due purely to the nanocrystalline milled state. If so, it is likely to be sintering/recrystallisation 'within' agglomerates as distinct from true sintering between agglomerates. It is also possible that the low temperature compaction is due in part to the residual Fe. Fe could act as a sintering agent by plastic deformation and oxidation to $FeO \rightarrow Fe_3O_4 \rightarrow Fe_2O_3$. However, the dilatometry test of a sample milled with 3 wt% Fe added suggests that merely adding Fe to alumina powder and lightly co-milling is insufficient to promote sintering to a large degree. A small decrease in the sintering temperature when compared with the unmilled sample was observed, this could be due either to the 15 min of milling, or the added Fe, and cannot be determined at this stage. Given the rapid approach to the nanocrystalline state (Fig. 2), it appears as though it is the nanocrystalline state rather than the Fe that is responsible.

In the work presented here we have focussed on powder milled for 16 h. In this condition, the powders have the greatest Fe contamination. The milling induced crystallite size after 4 or even 2 h of milling may be almost equivalent to the final milled state, but with far less Fe (Fig. 2). However, if the lattice expansion during milling is due to defect formation, then Fig. 3 suggests far fewer defects have been created in the shorter milling times. Further work is required to disentangle the relative contributions of crystallite size, defects and Fe contamination.

Conclusions

1. High-energy mechanical milling readily produces nanocrystalline Al_2O_3.
2. When Fe-based milling media are used, Fe contaminates the Al_2O_3 approximately linearly with

milling time. This could be reduced by shorter milling times, but this may decrease the concentration of structural defects.
3. The alumina remains in the α-Al_2O_3 form, but with lattice expansion mainly due to vacancies and other structural defects.
4. A significant reduction in sintering temperature to below 1200 °C was realised.
5. The density of the milled and sintered samples was 94–96% of theoretical density, which is excellent for a low temperature pressure-less sintered alumina ceramic.

Acknowledgements The authors thank the Australian Research Council for financial support. We also thank Mr. David Phelan for assistance with the electron microscopy, and Mr. Peter Garfoot for his assistance with sample preparation.

References

1. Karagedov GR, Lyakhov NZ (1999) Nanostruct Mater 11(5):559
2. Cutler IV, Bradshaw C, Christensen CJ, Hyatt EP (1957) J Am Ceram Soc 40:134
3. Johnson WC, Coble RL (1978) J Am Ceram Soc 61:110
4. Inada S, Kimura T, Yamaguchi T (1990) Ceram Int 16:369
5. Sathiyakumar M, Gnanam FD (2002) Ceram Int 28:195
6. Erkalfa H, Misirli Z, Baykara T (1995) Ceram Int 21:345
7. Boccaccini AR, Kaya C (2002) Ceram Int 28:893
8. Shiau F-S, Fang T-T (1999) Mater Chem Phys 60:91
9. Pathak LC, Singh TB, Das S, Verma AK, Ramachandrarao P (2002) Mater Lett 57:380
10. Ananthapadmanabhan PV, Thiyagarajan TK, Sreekumar KP, Venkatramani N (2004) Scripta Mater 50:143
11. Park JH, Lee MK, Rhee CK, Kim WW (2004) Mater Sci Eng A 375–377:1263
12. Goldsby JC (2001) Ceram Int 27:701
13. Karagedov GR, Lyakhov NZ (2003) KONA 21:76
14. Howard CJ, Hunter BA (1997) A computer program for Rietveld analysis of X-ray, neutron diffraction patterns. ANSTO Lucas Heights Research Laboratories
15. Klug HP, Alexander LE (1974) X-ray diffraction procedures for polycrystalline and amorphous materials, 2nd edn. J. Wiley and Sons, New York, p 662
16. Hill RJ, Howard CJ (1987) J Appl Cryst 20:467
17. Alkebro J, Begin-Colin S, Mocellin A, Warren R (2000) J Europ Ceram Soc 20:2169